OAK RIDGE National Laboratory

Mass Accountancy with the MOLE/GRIFFIN Code for the Molten Salt Reactor Experiment

Kyoung O. Lee

ORNL is managed by UT-Battelle, LLC for the US Department of Energy

U.S. DEPARTMENT OF ENERGY

OAK RIDGE National Laboratory

Introduction to Mole Code

- **Mole** code is part of the Nuclear Energy Advanced Modeling and Simulation (NEAMS) program supported by US Department of Energy Office of Nuclear Energy.
- Mole code predicts the formation of fouling, erosion, and corrosion in molten salt reactor (MSR) fuel-cycle and flow loops with **thermophysical/themochemical properties and phase equilibrium/transitions**.
- Mole code performs macroscale/mesoscale diffusion or coupling with reactor codes to solve eigenvalue problems/transient analysis with improved fidelity capability for **MSR safety analysis**.
- **Decay and the transmutation of nuclides** can calculate the transition of the parent nucleus to a daughter nucleus of the static/dynamic radioisotopes.

Introduction to Mole Code (cont.)

Mole code

- Mole code includes the corrosion and leaching of chromium with heat conduction.
- Mole code focuses on **noble metals and noble gases**.

Salt Dynamics

- Solid alloy
  - Macroscopic description of diffusion in the solid alloy below the surfaces
- Surface interface in liquid solution
  - Electrochemical surface reaction
  - Solid to liquid solution for convective mass transfer
  - Liquid solution to solid for convective mass transfer
- Salt interface in liquid-gas transition
  - **Liquid solution to gas (vapor)** for convective mass transfer
  - **Gas to liquid** or depositions on wall for convective mass transfer
- Nuclear transmutation and radioactivity
  - Bateman equations with fission fragments and neutron sources

Nuclear Energy Advanced Modeling and Simulation (NEAMS), DOE-NE

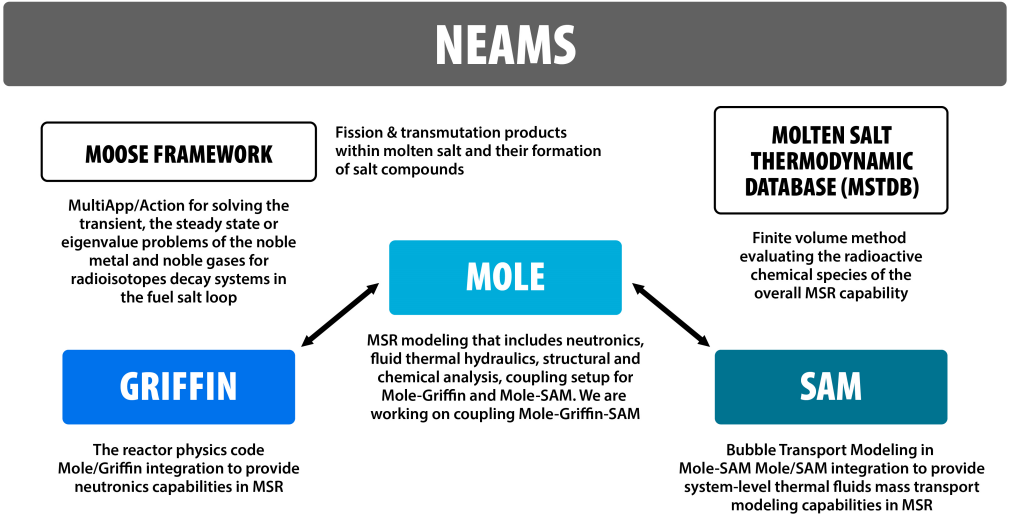

Delayed Neutron Precursors in MSRE

- This work investigates the delayed neutron precursors with advection from the fission of ^{235}U in molten salt reactors.
- The six delayed neutron groups predict the spatial distribution by the advective transport for radioactive mass transfer in the Molten-Salt Reactor Experiment (MSRE).
- Mole, using the framework of the Multiphysics Object-Oriented Simulation Environment (MOOSE), was used to compute the delayed neutron concentration of the whole system.
- This approach can be used for analysis of reactivity in circulating conditions. The effect of delayed neutron concentrations on the static or dynamic behavior of the system in MSRE was analyzed.

Molten-Salt Reactor Experiment

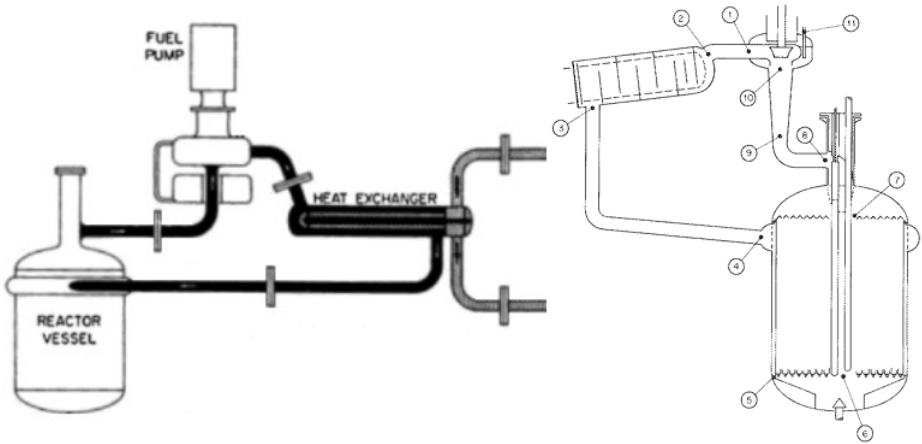

Figure 1: Schematic diagram of a reactor vessel with external loop for fuel salt circulation for MSRE Assembly

MSRE System

Table 1: Volumes, residence time, and fluid velocity in fuel circulating loop of MSRE

	Volume (ft^3)	Residence Time (sec)	Length (cm)	Fluid velocity † (cm/sec)	(ft/sec)
Pump $^{10\to1}$	1.10	0.41	56.6	149.4	4.90
Fuel Loop Piping $^{1\to2}$	0.76	0.28	39.1	149.4	4.90
Heat Exchanger $^{2\to3}$	6.12	2.29	589.7	279.6	9.17
Fuel Loop Piping, $^{3\to4}$	2.18	0.81	112.2	149.4	4.90
Outer annulus, $^{4\to5}$	9.72	3.63	157.9	47.1	1.55
Lower plenums, $^{5\to6}$	12.24	4.58	18.1	29.9	0.14
Reactor vessel core, $^{6\to7}$	23.52	8.79	149.8	18.5	0.61
Upper plenums, $^{7\to8}$	11.39	4.26	17.4	29.9	0.15
Fuel Loop Piping, $^{8\to9}$	1.37	0.51	70.5	149.4	4.90
Fuel Loop Piping, $^{9\to10}$	0.73	0.27	37.6	149.4	4.90
Total	69.13	25.86	1,249.0		

† Volumetric flow rate, 1200 gpm is $Q = A_{\text{eff}}\mathbf{u}$, where A_{eff} is the effective cross section and $\mathbf{u}$ is fluid velocity.

Delayed Neutron Precursors in MSRE (cont.)

- Molten salt reactors (MSRs) use liquid fuels passing through a graphite-moderated reactor in a primary loop cycle of uranium tetrafluoride ($\mathrm{UF_4}$) dissolved in the mixture of lithium beryllium fluoride (FLiBe) and zirconium fluoride ($\mathrm{ZrF_4}$) and a secondary loop cycle using FLiBe salt coolant.
- This reactor concept features circulating dynamic liquid fuels rather than static solid fuels. MSRs have safety and sustainability advantages over conventional nuclear reactors.
- The Molten-Salt Reactor Experiment (MSRE) was a research reactor operating from 1966 to 1969 using molten fluoride salts at Oak Ridge National Laboratory (ORNL).
- The fuel salt operating temperature of 1,200°F (648.9°C) was circulated through the reactor vessel heated by the fission chain reaction, and the heat exchanger transferred to the coolant salts in an independent loop.

The Spectrum of Neutron Flux

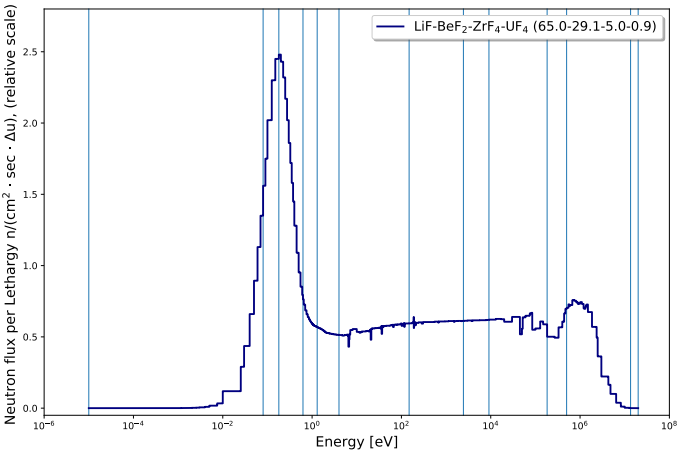

Figure 2: Neutron flux per unit lethargy on semi-log x-axis for $\mathrm{LiF\text{-}BeF_2\text{-}ZrF_4\text{-}UF_4}$ (65.0-29.1-5.0-0.9) and vertical lines represent 11 energy groups from Shift neutron flux

The Spectrum of Neutron Flux (cont.)

- The neutron flux per lethargy was performed for the full design of the MSRE using Shift/MPACT. Our results obtained from Shift/MPACT for the MSRE are in good agreement with the MSRE spectrum of the reference.
- The spectrum of neutron flux can be evaluated for fast and thermal neutron distribution in the core. Thus, the delayed neutron precursors will be investigated in two parts: thermal neutrons and fast neutrons.
- The steady-state one-group neutron diffusion equation is coupled with six-group delayed neutron concentration equations at the initial threshold ^{235}U because of the fuel cycle.
- The static and dynamic reactivity are determined for the circulation operations. This work includes a comparison of the corresponding neutrons calculated from the theoretical model with the results of the MSRE data.
- This work describes a method for Mole—an application code in the Multi-Physics Object Oriented Simulation Environment (MOOSE) framework—to take into account the neutron transport for delayed neutron precursors.

The parameters and physical properties of MSRE

Table 2: The parameters and physical properties of MSRE

Reactor designed power	10.0 Mw (thermal)	
Reactor operating power	7.3 Mw (thermal)	
	US Measure	SI Units
Primary Loop		
LiF-BeF_2-ZrF_4-UF_4 (65.0-29.1-5.0-0.9) %aw		
Liquidus Temperature	813°F	707.04 K (433.89°C)
Fuel salt flow rate	1,200 gpm	0.07571 m^3/sec
Temperature, Fuel inlet reactor vessel	1,175°F	908.15 K (635.00°C)
Temperature Fuel outlet reactor vessel	1,225°F	935.93 K (662.78°C)
Reactor Vessel		
Diameter of graphite moderated region	55.0 in.	1.3970 m
Height of graphite moderated region	64.0 in.	1.6256 m
Circulating primary salt volume	69.13 ft^3	1.9575 m^3
Reactor vessel core	23.52 ft^3	0.6660 m^3
Heat exchanger	6.12 ft^3	0.1733 m^3
Outer annulus, the lower and upper plenums	33.35 ft^3	0.9444 m^3
Pump and piping	6.14 ft^3	0.1739 m^3
Secondary Loop, Heat Exchanger		
LiF-BeF_2 (64-34) at. wt %		
Coolant salt flow rate	850 gpm	0.05363 m^3/sec
Temperature Heat exchanger inlet	1,025°F	824.82 K (551.67°C)
Temperature Heat exchanger outlet	1,100°F	866.48 K (593.33°C)
Effective surface	259 ft^2	24.0619 m^2

Delayed Neutron Data

The delayed neutrons are emitted by an excited fission product nucleus during beta minus decay. Many decay chains are important for delayed neutron emission. Therefore, delayed neutrons are generally classified into six groups. Keepin's fission data of thermal and fast neutron $^{235}\mathrm{U}$ were used, and Keepin's data for six-group delayed neutron parameters have proven to perform well.

Table 3: Delayed neutron data for six-group precursor of thermal and fast fission $^{235}\mathrm{U}$

	thermal fission $^{235}\mathrm{U}$			fast fission $^{235}\mathrm{U}$		
Group index i	Half-Life (sec), $\mathrm{T}_{1/2}$	$\lambda\ (s^{-1})$	β_i	Half-Life (sec), $\mathrm{T}_{1/2}$	$\lambda\ (s^{-1})$	β_i
1	55.72	0.01244	0.000211	54.51	0.01272	0.000247
2	22.72	0.03051	0.001402	21.84	0.03174	0.001385
3	6.22	0.11144	0.001254	6.00	0.11552	0.001222
4	2.30	0.30137	0.002528	2.23	0.31083	0.002645
5	0.610	1.13631	0.000740	0.496	1.39747	0.000832
6	0.230	3.01368	0.000270	0.179	3.87233	0.000169

Time-dependent Neutron Transport Equations

The time-dependent neutron transport equations for the prompt neutron flux, ϕ, and the delayed neutron precursors, C_i, with drift in MSRs are written as

$$\frac{1}{v}\frac{\partial \phi}{\partial t} - \nabla \cdot (D\nabla\phi) + \Sigma_a \phi = (1-\beta)\,\nu\Sigma_f \phi + \sum_i^{I_N} \lambda_i C_i, \tag{1}$$

$$\frac{\partial C_i}{\partial t} + \nabla \cdot (\mathbf{u} C_i) = -\lambda_i C_i + \beta_i \nu \Sigma_f \phi, \quad i = 1, \ldots, I_N, \tag{2}$$

- v is the neutron velocity, $\mathbf{u}$ is the liquid fuel velocity, D is the neutron diffusion coefficient,
- Σ_f is the macroscopic fission cross section, ν is the average number of neutrons emitted per fission reaction, and Σ_a is the macroscopic absorption cross section.
- $\beta = \sum \beta_i$, where β_i is the each group delayed neutron fraction emitted per fission of precursor group i. $\beta = \nu_d/(\nu_p + \nu_d)$, where ν_d and ν_p are the delayed and prompt neutrons produced per fission.
- a decay constant λ_i, and the half-life of the neutron precursor of i.

1D delayed neutron calculation

The neutron flux via the method of separation of variables in a cylindrical reactor is given by $\phi(r,z) \sim J_0(2.405r/\widetilde{\mathrm{R}})\sin(\pi z/\widetilde{\mathrm{H}})$; $\widetilde{\mathrm{R}}$ is the extrapolated radius of the core, and $\widetilde{\mathrm{H}}$ is the extrapolated height of the core. The radial flux has the shape of J_0, the Bessel function of the first kind of order zero, and the axial flux has the shape of a sine in z axis direction. Thus, the flux is $\phi(z) = \phi_0 \sin(\pi z/\widetilde{\mathrm{H}})$. For 1D delayed neutron calculations, we can express this approximation as the following equation:

$$\frac{\partial C_i}{\partial t} + \frac{\partial (u_x C_i)}{\partial x} = -\lambda_i C_i + \beta_i \nu \Sigma_f \phi_0 \sin(\pi x/\widetilde{\mathrm{H}}), \tag{3}$$

where $x \in [0, \widetilde{\mathrm{H}}]$ for $\sin(\pi x/\widetilde{\mathrm{H}})$, otherwise zero. The superficial velocity of a salt fluid is defined as the volumetric flow rate of that fluid divided by the effective cross sectional area of a cylinder. The extrapolated height $\widetilde{\mathrm{H}}$ follows the sum of lengths from lower plena to upper plena $^{5\to6\to7\to8}$ in Table 1.

Time Scale of Thermal and Fast ^{235}U

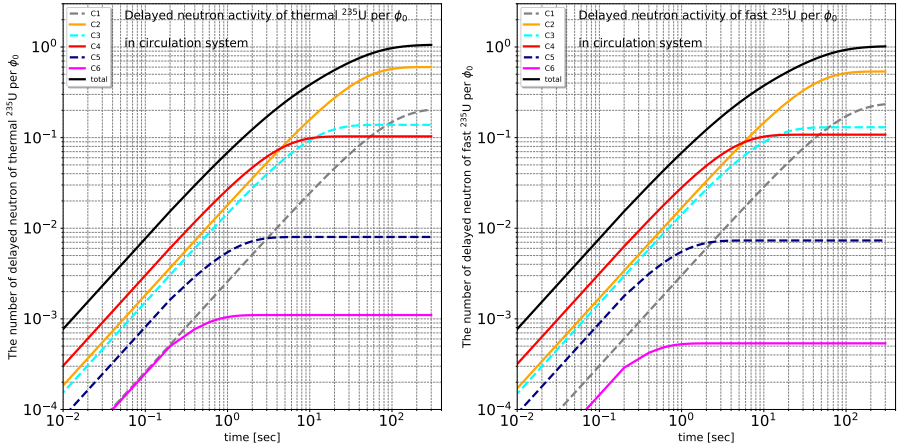

Figure 3: The six-group delayed neutron precursors of thermal and fast ^{235}U as a function of time up to 300 sec

DNP Spatial Distribution of 1st cycle, Thermal ^{235}U

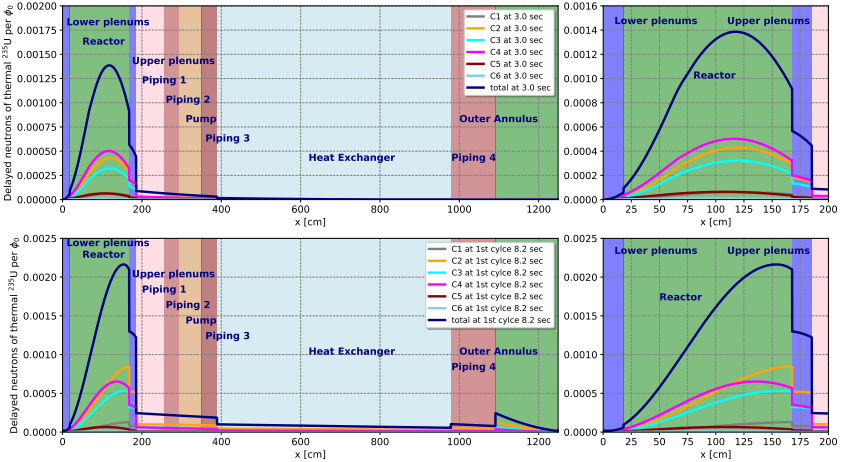

Figure 4: The spatial distribution of each six-group delayed neutron precursor of thermal ^{235}U at 3 sec (upper) and 1st cycle (lower)

DNP Spatial Distribution of 1st cycle, Fast ^{235}U

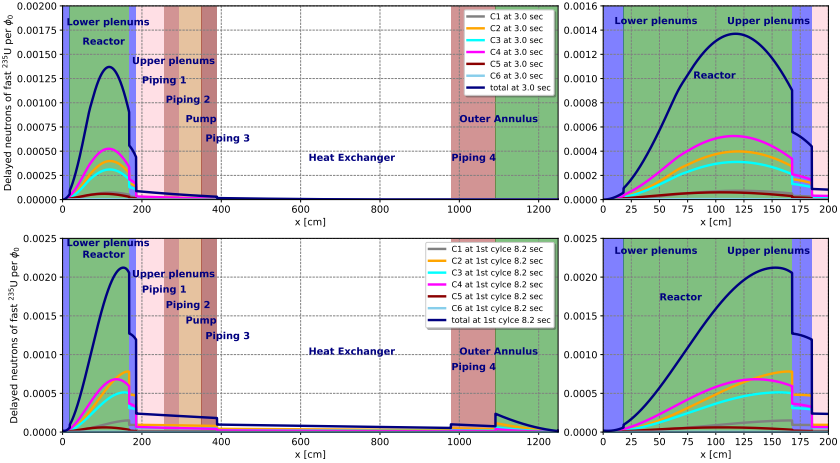

Figure 5: The spatial distribution of each six-group delayed neutron precursors of fast ^{235}U at 3 sec (upper) and 1st cycle (lower)

DNP Spatial Distribution of Thermal ^{235}U, 1st to 12th Cycle

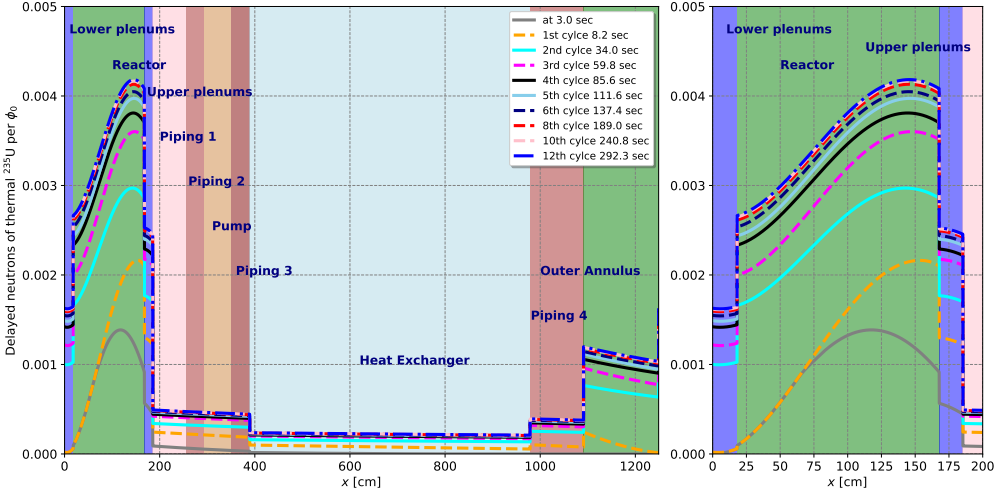

Figure 6: The spatial distribution of total yield of six-group delayed neutron precursors of thermal ^{235}U from 1^{st} to 12^{th} cycle

DNP Spatial Distribution of Fast ^{235}U, 1st to 12th Cycle

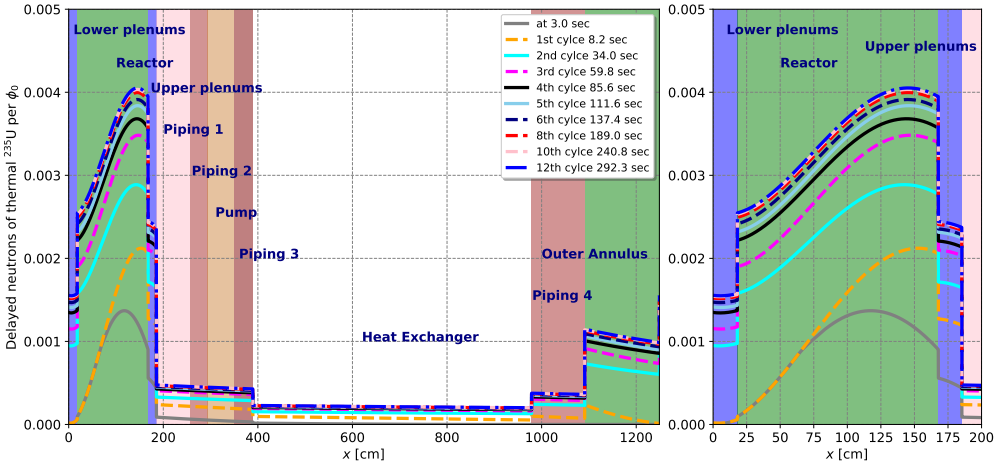

Figure 7: The spatial distribution of total yield six group delayed neutron precursors of fast ^{235}U from 1^{st} to 12^{th} cycle

DNP with/without Advection of Thermal and Fast ^{235}U at 300 secs

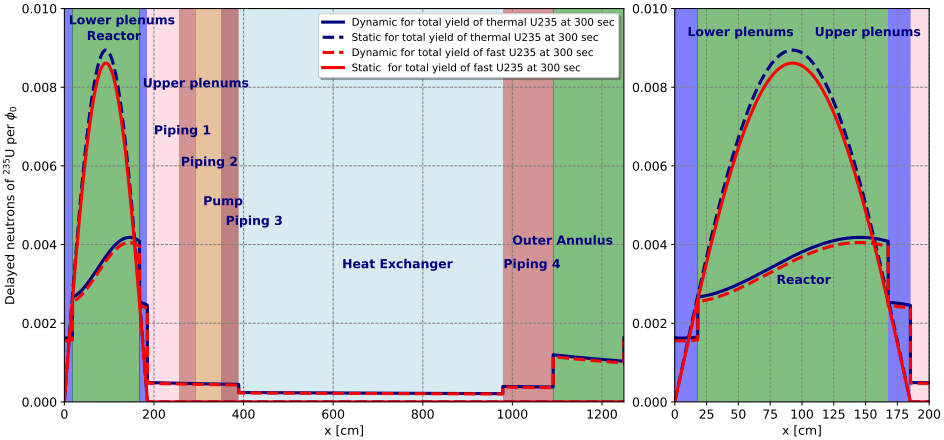

Figure 8: The static and dynamic spatial distribution of total yield of six-group delayed neutron precursors of thermal and fast ^{235}U at 300 secs

Coupling Mole-Griffin, Transient state

The prompt neutron diffusion equation is

$$\frac{1}{v_g}\frac{\partial \phi_g}{\partial t} - \nabla \cdot (D_g \nabla \phi_g) + \Sigma_{r,g}\phi_g = \sum_{\substack{g'=1 \\ g' \neq g}}^{G} \Sigma_s^{g' \to g}\phi_{g'} + (1-\beta)\,\chi^{p,g} \sum_{g'=1}^{G} \nu\Sigma_{f,g'}\phi_{g'} + \sum_{i}^{I_N} \chi_i^{d,g}\lambda_i C_i$$

The delayed neutron precursors equation is

$$A\frac{\partial C_i}{\partial t} + \nabla \cdot (A\mathbf{u}C_i) = -A\lambda_i C_i + A\beta_i \sum_{g'=1}^{G} \nu\Sigma_{f,g'}\phi_{g'}, \quad i = 1, \ldots, I_N$$

where β is not effective delayed neutron fraction.
$\nu = \nu_p + \nu_d$, $\nu_p = \nu(1-\beta)$ and $\beta = \nu_d/\nu = \sum_i \beta_i$

Coupling Mole-Griffin, Eigenvalue and Steady state

The prompt neutron diffusion equation is

$$-\frac{\partial}{\partial x}\left(D_g\frac{\partial}{\partial x}\phi_g\right)+\Sigma_{t,g}\phi_g=\sum_{g'=1}^{G}\Sigma_s^{g'\to g}\phi_{g'}$$
$$+\frac{1}{k_{\text{eff}}}\sum_{g'=1}^{G}\chi^{p,g,g'}\left(1-\beta_{g'}\right)\nu_{g'}\Sigma_{f,g'}\phi_{g'}+\sum_{i=1}^{I_N}\chi_i^{d,g}\lambda_i C_i$$

The delayed neutron precursors equation is

$$\frac{\partial}{\partial x}\left(Au_xC_i\right)=-A\lambda_iC_i+A\frac{\beta_i}{k_{\text{eff}}}\sum_{g'=1}^{G}\nu_{g'}\Sigma_{f,g'}\phi_{g'},\quad i=1,\ldots,I_N,$$

where β is not effective delayed neutron fraction.
$\nu=\nu_p+\nu_d$, $\nu_p=\nu(1-\beta)$ and $\beta=\nu_d/\nu=\sum_i\beta_i$

DNP Spatial Distribution for Eigenvalue -Steady State

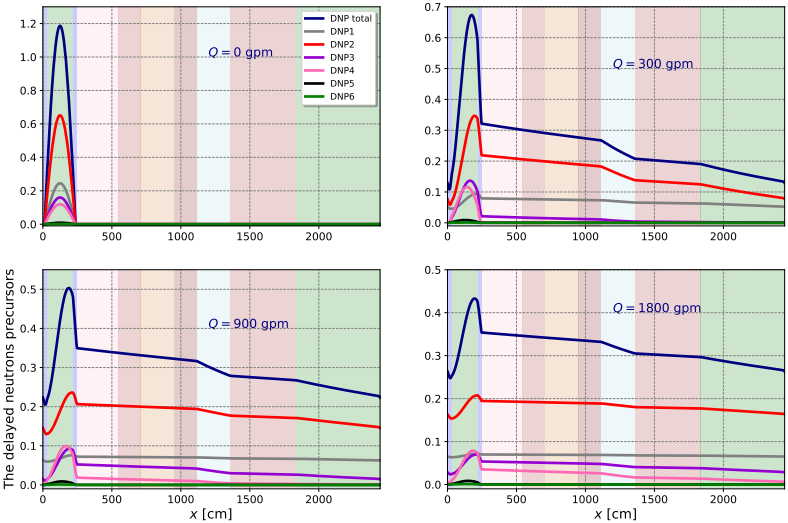

Figure 9: The spatial distribution of total yield six group delayed neutron precursors

DNP Spatial Distribution for Eigenvalue -Steady State

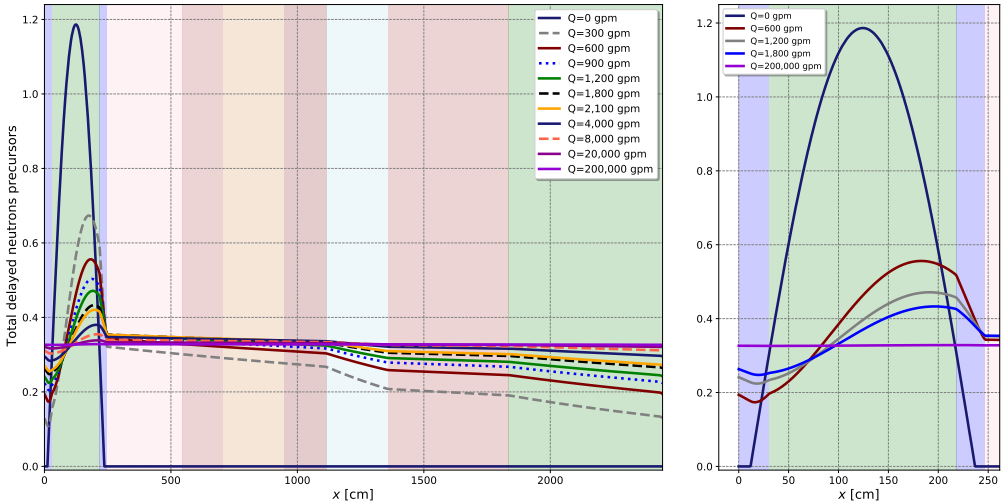

Figure 10: The spatial distribution of total yield six group delayed neutron precursors

Fission spectrum with advection

Total fission spectrum with/without advection is

$$\chi^* = (1-\beta)\,\chi_p + \sum_{i=1}^{I_N} \chi_i^d \left[1 - \exp\left(-\frac{\lambda_i}{u_x} x\right)\right] \beta_i \tag{4}$$

$$\chi = (1-\beta)\,\chi_p + \sum_{i=1}^{I_N} \chi_i^d \beta_i \tag{5}$$

The β_{eff} from the Keepin definition can use Bretscher's approximation

$$\beta_{\text{eff}} = \sum_{i}^{I_N} \beta_{\text{eff},i} = \frac{< \phi^\dagger \chi_d^* \beta \nu \Sigma_f \phi >}{< \phi^\dagger \chi^* \nu \Sigma_f \phi >} \cong 1 - \frac{k_p}{k_{\text{eff}}} \tag{6}$$

The eigenvalues of k_p and k_{eff} for steady-state are expressed using the bra–ket notation of the adjoint neutron flux

$$k_p = \frac{< \phi_p^\dagger \chi_p \nu_p \Sigma_f \phi_p >}{< \phi_p^\dagger \widehat{M} \phi_p >} \qquad k_{\text{eff}} = \frac{< \phi^\dagger \chi^* \nu \Sigma_f \phi >}{< \phi^\dagger \widehat{M} \phi >} \tag{7}$$

k_{eff} and β_{eff} according to the flow rate

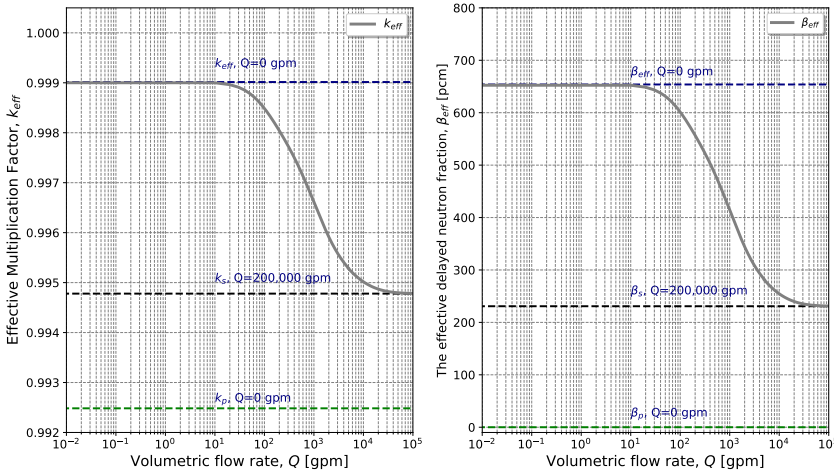

Figure 11: k_{eff} and β_{eff} according to the flow rate

k_{eff} and β_{eff} according to the flow rate

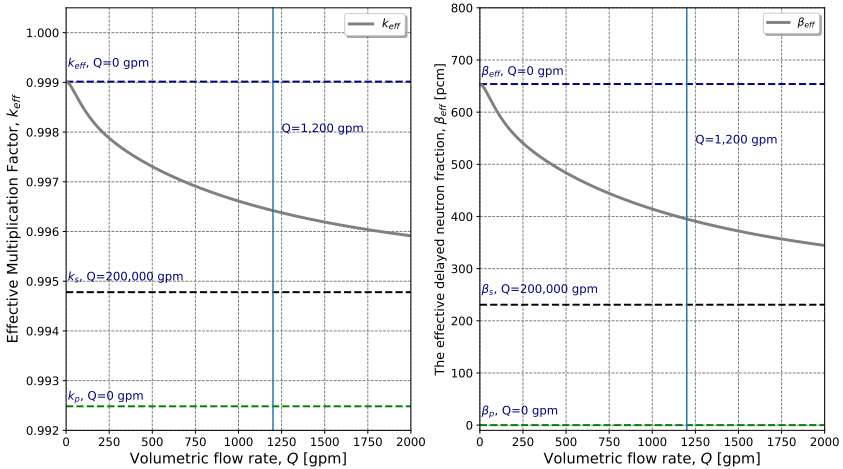

Figure 12: k_{eff} and β_{eff} according to the flow rate

Mass Transfer across a Gas–Liquid Interface

There are two film theories and the overall mass transfer coefficients

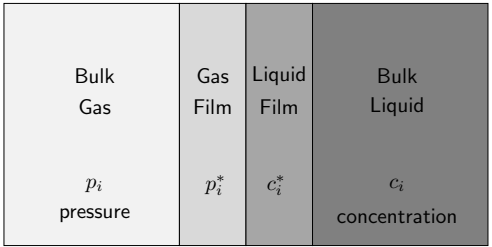

$$c_i^* = p_i H$$

$$p_i^* = c_i / H$$

Figure 13: The gas–liquid interface of the film theory expressed in partial pressures and concentrations.

Liquid transport:

$$\frac{\partial c_l}{\partial t} + \nabla \cdot \mathbf{J}_l = K_L a \left(c_l^* - c_l\right)$$

$$\mathbf{J}_l = -D_l \nabla c_l - \mathbf{u} c_l$$

Gas transport:

$$\frac{\partial c_g}{\partial t} + \nabla \cdot \mathbf{J}_g = K_G a \left(p_g - p_g^*\right)$$

$$\mathbf{J}_g = -D_g \nabla c_g - \mathbf{v} c_g$$

K_G is the overall gas-phase mass transfer coefficient, K_L is the overall liquid-phase mass transfer coefficient, $\mathbf{u}$ is liquid velocity, $\mathbf{v}$ is gas velocity, and H is Henry's gas constant. a is gas–liquid interfacial area per unit volume, and D is diffusivity.

Mass Transfer across a Gas–Liquid Interface (cont.)

The overall mass transfer coefficients, K_G — gas phase and K_L — liquid phase are defined as:

$$\frac{1}{K_G} = \frac{1}{k_l H} + \frac{1}{k_g} \qquad \frac{1}{K_L} = \frac{1}{k_l} + \frac{H}{k_g}$$

where k_l is the liquid phase mass transfer coefficient and k_g is the gas phase mass transfer coefficient. H is Henry's Law constant and defined by $H = c_l/p_g$.
The entropy change for an equilibrium process can be explained by the Gibbs free energy.

$$\Delta G = \Delta \mathcal{H} - T\Delta S$$

where $\Delta\mathcal{H}$ is enthalpy change, ΔS is entropy change, and T is temperature in K. When the temperature of a system changes, Henry's constant changes and is related to the Van 't Hoff equation. The least squares regression can find the arbitrary numbers, α and β.

$$\Delta G = RT \ln H = \alpha 4\pi r^2 \gamma + \beta$$

where R is the ideal gas constant, r is the van der Waals radius, and γ is the surface tension.

Henry's gas constant

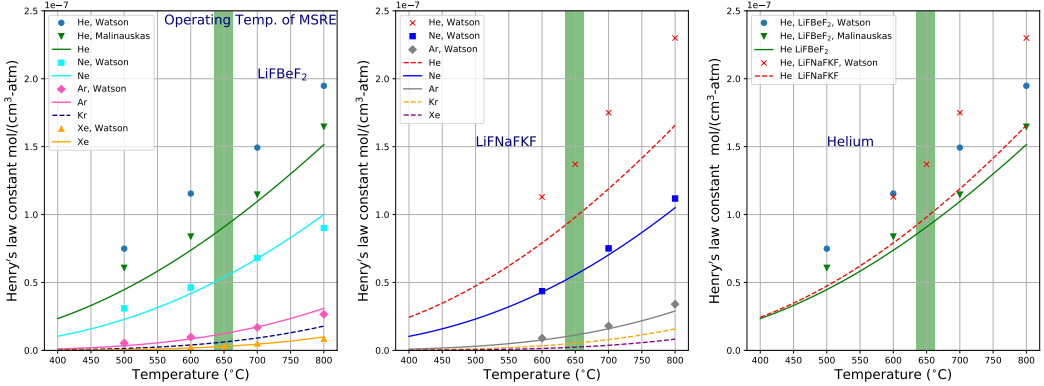

Figure 14: Henry's gas constant dependent on temperature (left $\mathrm{LiF\text{-}BeF_2}$; right $\mathrm{LiF\text{-}NaF\text{-}KF}$)

Liquid Salt Thermophysical and Thermochemical Properties

- $LiF\text{-}BeF_2$ (64.0-36) at. wt%.
  $\gamma(T) = 235.5 - 0.09T(^\circ\mathrm{C})[\mathrm{erg/cm^2}]$
  $\rho_f(T) = 2.09 - 2.7 \times 10^{-4} T(^\circ\mathrm{C})[\mathrm{g/cm^3}]$
  $\mu_f(T) = 0.0594 \exp\left[4605/T(^\circ\mathrm{K})\right][\mathrm{mPa-s}]$

- LiF-NaF-KF (46.5-11.5-42.0) at. wt%.
  $\gamma(T) = 237.0 - 0.0788T(^\circ\mathrm{C})[\mathrm{erg/cm^2}]$
  $\rho_f(T) = 2.47 - 0.68 \times 10^{-3} T(^\circ\mathrm{C})[\mathrm{g/cm^3}]$
  $\mu_f(T) = 0.04 \exp\left[4170/T(^\circ\mathrm{K})\right][\mathrm{mPa-s}]$

- Liquid–Mass diffusivity: Stokes–Einstein and the Wilke–Chang equations, and Hayduk-Minhas correlation

$$D = \frac{k_B T(^\circ\mathrm{K})}{6\pi\mu_f r_0} \quad \text{or} \quad \frac{7.4 \times 10^{-8}(\phi M)^{0.5} T(^\circ\mathrm{K})}{\mu_f V_B^{0.6}}[\mathrm{m^2/sec}] \quad \text{or} \quad 13.3 \times 10^{-8} \frac{T^{1.47}\mu_f^{\epsilon}}{V_b^{0.71}}$$

$$\epsilon = 10.2/V_b - 0.791$$

where k_b is the Boltzmann constant, r_0 is the solute radius, M is the molecular weight solvent, V_B is the molar volume at boiling point, and ϕ is the factor for solute.

Dittus–Boelter Equation: Turbulent Flow

The Dittus–Boelter equation in circular tubes is:

$$\mathrm{Sh} \ = 0.023 \mathrm{Re}^{0.8} \mathrm{Sc}^{n} = \frac{h_c L}{D},$$

where:
$n = 0.4$ for heating, $n = 0.3$ for cooling,
L is a cylinder diameter,
D is the diffusivity, and
turbulent flow, $\mathrm{Re} >$ 10,000

$$\mathrm{Re} = \frac{\rho_f \left|\mathbf{u}\right| L}{\mu_f} = \frac{\rho_f Q L}{\mu_f A} \qquad \text{Reynolds number}$$

$$\mathrm{Sc} = \frac{\mu_f}{\rho_f D} \qquad \text{Schmidt numbers}$$

$$\mathrm{Sh} = \frac{h_c L}{D} \qquad \text{Sherwood number}$$

where: ρ_f is the density of the fluid,
μ_f is the dynamic viscosity of the fluid, and
$\mathbf{u}$ is the velocity of the fluid

- The mass transfer coefficient k is

$$k = 0.023 \frac{D}{L} \mathrm{Re}^{0.8} \mathrm{Sc}^{n}$$

Liquid–Gas Mass Transport Using Mole

We have considered the mechanism of mass transfer between phases without convection. The overall mass transfer coefficients were defined by $c_l = p_g H = c_g HRT$ and $K_G = K_L H$, where $p_g = c_g RT$ and $R = 82.05746[\mathrm{cm}^3 \cdot \mathrm{atm}/(\mathrm{K} \cdot \mathrm{mole})]$.

$$\text{Liquid transport:}$$

$$\frac{\partial c_l}{\partial t} = K_L a \left(c_g HRT - c_l \right)$$

$$\text{Gas transport:}$$

$$\frac{\partial c_g}{\partial t} = K_G a \left(c_g RT - c_l / H \right)$$

where c is the concentration of species in liquid, p is the partial pressure of species in gas phase, and H is Henry's gas constant. a is the gas–liquid interfacial area per unit volume.

$LiBeF_2$

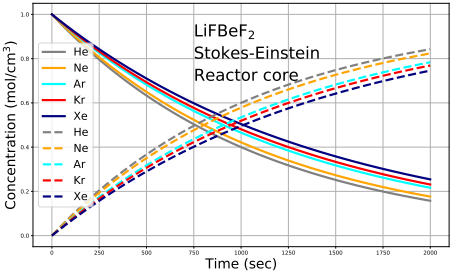
LiFBeF2
Stokes-Einstein
Reactor core
Concentration (mol/cm3)
Time (sec)
He
Ne
Ar
Kr
Xe

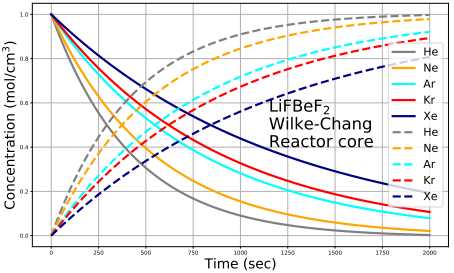
LiFBeF2
Wilke-Chang
Reactor core
Concentration (mol/cm3)
Time (sec)
He
Ne
Ar
Kr
Xe

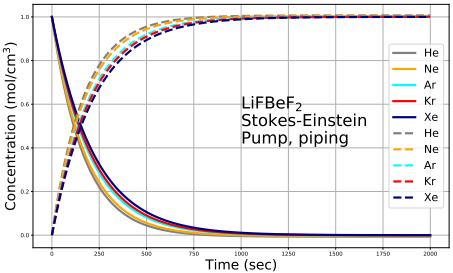
LiFBeF2
Stokes-Einstein
Pump, piping
Concentration (mol/cm3)
Time (sec)
He
Ne
Ar
Kr
Xe

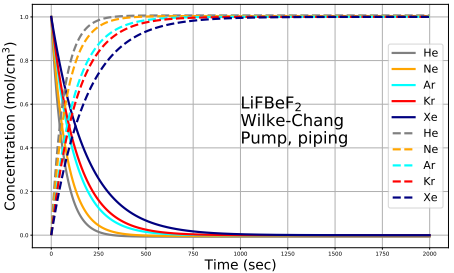
LiFBeF2
Wilke-Chang
Pump, piping
Concentration (mol/cm3)
Time (sec)
He
Ne
Ar
Kr
Xe

LiFNaFKF

Initial constions: liquid 1 mole, gas 0 mole

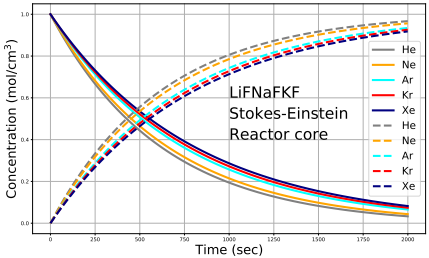

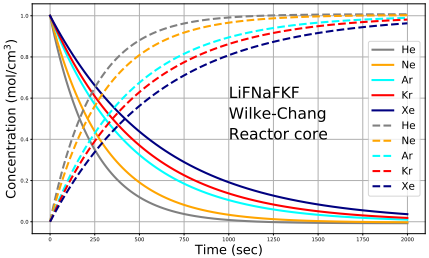

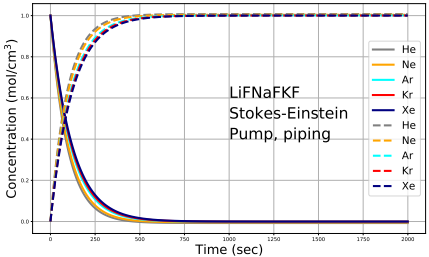

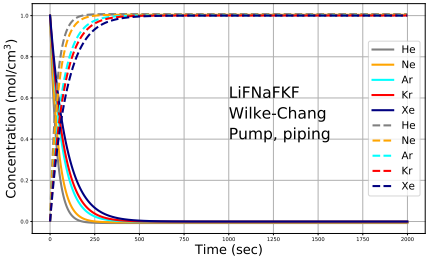

Table 4: MSRE Parameters

	Mass Transfer Coefficient (ft/hr)	Surface Area (ft^2)	Rate (hr^{-1})†
Heat Exchanger	0.550	315	2.457
Fuel Loop Piping, Core and Pump Volute	1.230	71	1.239
Core Wall Cooling Annulus	0.510	154	1.114
Core Graphite (Exposed to salt)	0.063	1465	1.309
Miscellaneous (10% of total products)			0.610
Summation with no bubble[a]			6.729
Bubbles of 233U Runs[b]	5.000	5581.00	395.816
Bubbles of 235U Runs[c]	5.000	345.00	24.468
Fuel Salt During the 233U Runs[a+b]			402.545
Fuel Salt During the 235U Runs[a+c]			31.197

† Mass transfer rate is $\kappa = h\dfrac{a}{V}$, where the volume of a fuel salt in the fuel loop is 70.5 ft^3

The columns of gray color are the data from Kedl's paper.

Noble Metals

Table 5: Noble Metals For the 233-U and 235-U Runs

233-U	Direct Yield of Noble Metal %	Half Life	Decay Rate (hr^{-1})	Precursor	Cumulative Yield of Precursor %	Half Life	Decay Rate (hr^{-1})
$^{99}_{42}\mathrm{Mo}$	0.00	65.924 hrs	1.0514×10^{-2}	$^{99}_{41}\mathrm{Nb}$	4.8900	2.5 mins	16.6355
$^{103}_{44}\mathrm{Ru}$	0.00	39.247 days	7.3588×10^{-4}	$^{103}_{43}\mathrm{Tc}$	2.0000	54.2 sec	46.0393
$^{105}_{44}\mathrm{Ru}$	0.00	4.44 hrs	1.5611×10^{-1}	$^{105}_{43}\mathrm{Tc}$	0.7060	7.6 mins	5.4722
$^{106}_{44}\mathrm{Ru}$	0.00	371.8 days	7.7679×10^{-5}	$^{106}_{43}\mathrm{Tc}$	0.4380	35.6 sec	70.0935
$^{125}_{51}\mathrm{Sb}$	0.00	2.75856 yrs	2.8684×10^{-5}	$^{125}_{50}\mathrm{Sn}$	0.0839	9.64 days	0.0030
$^{127}_{51}\mathrm{Sb}$	0.00	3.85 days	7.5016×10^{-3}	$^{127}_{50}\mathrm{Sn}$	0.5800	2.1 hrs	0.3301
$^{129m}_{52}\mathrm{Te}$	0.00	33.6 days	8.5956×10^{-4}	$^{129}_{51}\mathrm{Sb}$	0.7100	4.366 hrs	0.1588
$^{131m}_{52}\mathrm{Te}$	0.00	33.25 hrs	2.0847×10^{-2}	$^{131}_{51}\mathrm{Sb}$	0.4410	23.03 mins	1.8059
$^{132}_{52}\mathrm{Te}$	0.00	3.204 days	9.0141×10^{-3}	$^{132}_{51}\mathrm{Sb}$	4.4300	2.79 mins	14.9064
$^{95}_{41}\mathrm{Nb}$	0.00	34.991 days	8.2541×10^{-4}	$^{95}_{40}\mathrm{Zr}$	6.0000	64.032 days	0.0005
Summation of Products			2.0652×10^{-1}				155.4451

235-U	Direct Yield of Noble Metal %	Half Life	Decay Rate (hr^{-1})	Precursor	Cumulative Yield of Precursor %	Half Life	Decay Rate (hr^{-1})
$^{99}_{42}\mathrm{Mo}$	0.00	65.924 hrs	1.0514×10^{-2}	$^{99}_{41}\mathrm{Nb}$	6.06	2.5 mins	16.6355
$^{103}_{44}\mathrm{Ru}$	0.00	39.247 days	7.3588×10^{-4}	$^{103}_{43}\mathrm{Tc}$	3.00	54.2 sec	46.0393
$^{106}_{44}\mathrm{Ru}$	0.00	371.8 days	7.7679×10^{-5}	$^{106}_{43}\mathrm{Tc}$	0.39	35.6 sec	70.0935
$^{129m}_{52}\mathrm{Te}$	0.00	33.6 days	8.5956×10^{-4}	$^{129}_{51}\mathrm{Sb}$	0.71	4.366 hrs	0.1588
$^{132}_{52}\mathrm{Te}$	0.00	3.204 days	9.0141×10^{-3}	$^{132}_{51}\mathrm{Sb}$	4.71	2.79 mins	14.9064
$^{95}_{41}\mathrm{Nb}$	0.00	34.991 days	8.2541×10^{-4}	$^{95}_{40}\mathrm{Zr}$	6.22	64.032 days	0.0005
Summation of Products			2.2027×10^{-2}				147.8340

The columns of gray color are the data from Kedl's paper and the data of half life is from ENSDF.

Fuel Salts For Nobel Metals (Liquid)

The Bateman Equations for Parent-daughter are

$A \longrightarrow B \longrightarrow$

$$\frac{\partial N_A}{\partial t} = R_A - \lambda_A N_A$$
$$\frac{\partial N_B}{\partial t} = R_B + \lambda_A N_A - k_B N_B$$

where $R_x = \gamma_x \Sigma_f \phi$, in which x means either A or B,
γ_x is cumulative yield fraction,
λ_A is the decay constant of the parent, and
$k_B = \lambda_B + \sum \kappa$ is the decay constant of the daughter and the summation of the mass transfer rate.

Fuel Salts For Nobel Metals (Liquid)

The analytic solutions are

$$
\begin{aligned}
N_A(t) &= N_{A0}\exp(-\lambda_A t) + R_A\left(\frac{1-\exp(-\lambda_A t)}{\lambda_A}\right) \\
N_B(t) &= N_{B0}\exp(-k_B t) + R_B\left(\frac{1-\exp(-k_B t)}{k_B}\right) \\
&\quad + N_{A0}\frac{\lambda_A}{k_B-\lambda_A}\left(\exp(-\lambda_A t)-\exp(-k_B t)\right) \\
&\quad + R_A\frac{\lambda_A}{k_B-\lambda_A}\left(\frac{1-\exp(-\lambda_A t)}{\lambda_A}-\frac{1-\exp(-k_B t)}{k_B}\right)
\end{aligned}
$$

where $N_A(0) \equiv N_{A0}$ and $N_B(0) \equiv N_{B0}$

Nobel Metals-233U without mass transfer

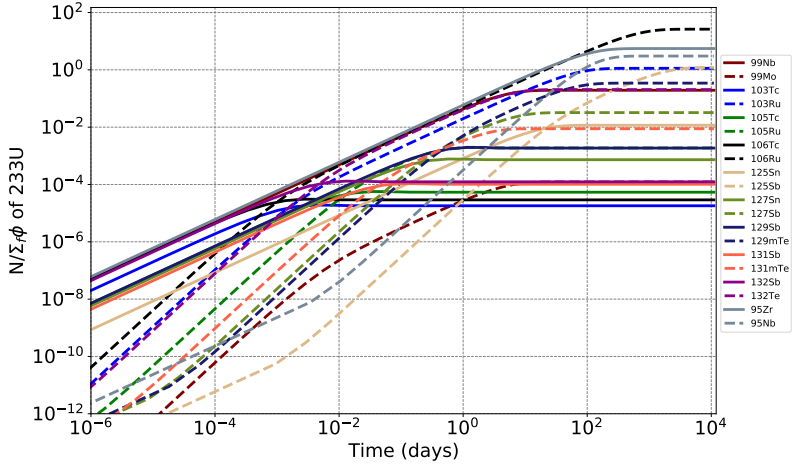

Figure 15: The ratio of the species numbers to $\Sigma_f \phi$ of 233U integrated into the whole system without mass transfer rate

Nobel Metals-233U with mass transfer

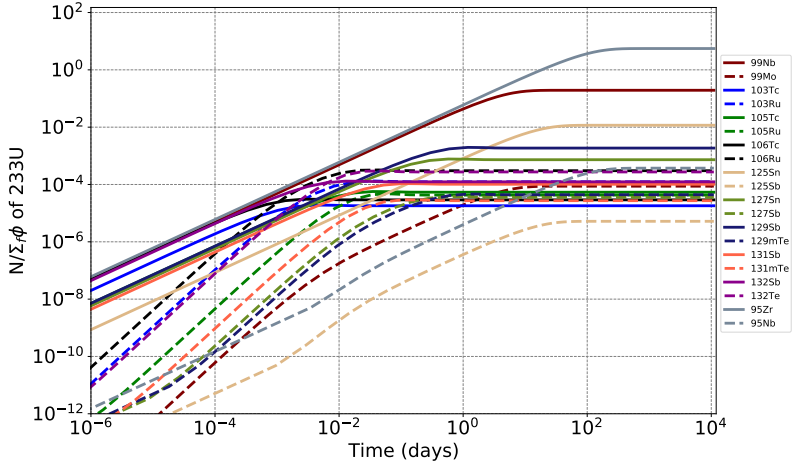

Figure 16: The ratio of the species numbers to $\Sigma_f \phi$ of 233U integrated into the whole system with mass transfer rate and bubble-free

Nobel Metals-233U with mass transfer and bubbles

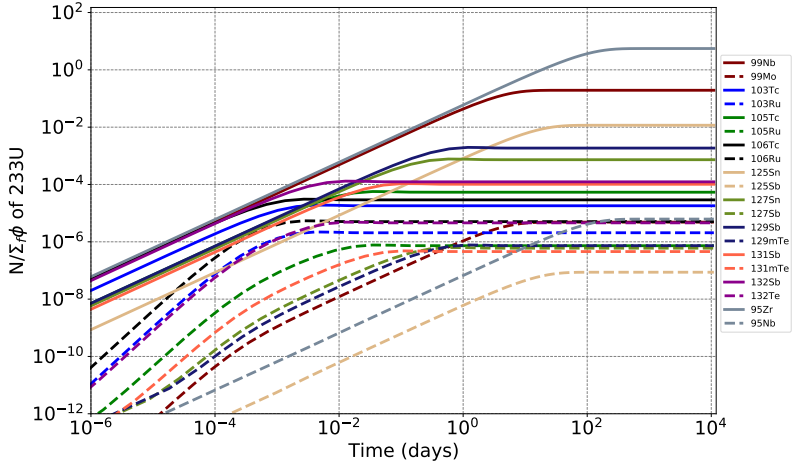

Figure 17: The ratio of the species numbers to $\Sigma_f \phi$ of 233U integrated into the whole system with mass transfer rate and bubbling

Nobel Metals-235U without mass transfer

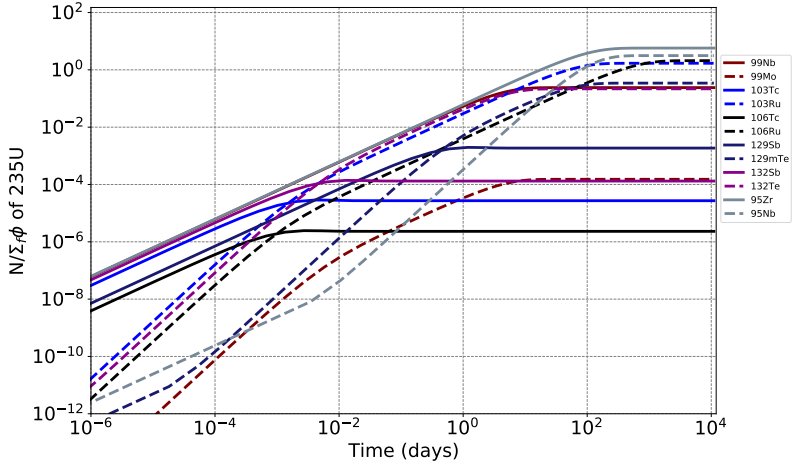

Figure 18: The ratio of the species numbers to $\Sigma_f \phi$ of 235U integrated into the whole system without mass transfer rate

Nobel Metals-235U with mass transfer

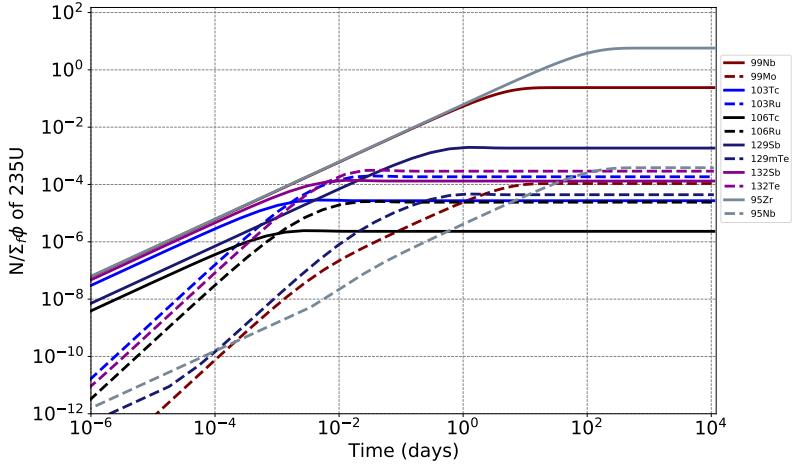

Figure 19: The ratio of the species numbers to $\Sigma_f \phi$ of 235U integrated into the whole system with mass transfer rate and bubble-free

Nobel Metals-235U with mass transfer and bubbles

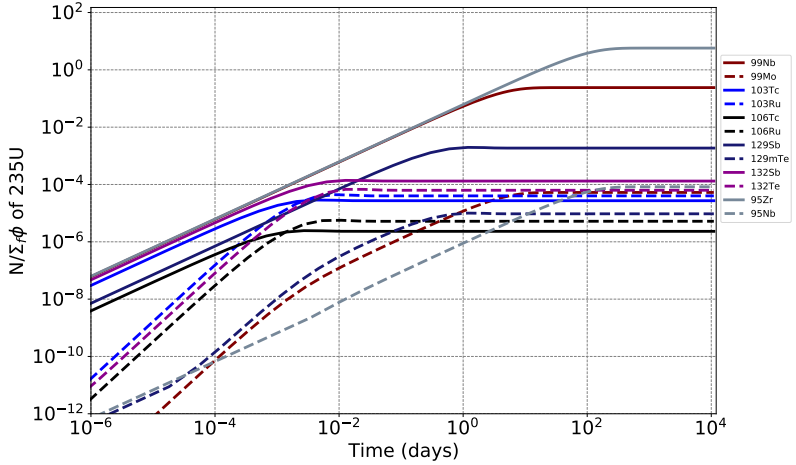

Figure 20: The ratio of the species numbers to $\Sigma_f \phi$ of 235U integrated into the whole system with mass transfer rate and bubbling

Summary

- The fast and thermal delayed neutron precursors are compared with the dynamics reactivity and static reactivity of the MSRE.
- The Mole code establishes periodic boundary conditions, which can continue to loop.
- The time of first cycle is 8.2 sec from outlet of upper plena to the inlet of outer annulus; otherwise, 25.86 sec is the entire loop cycling time. We found that the delayed neutron concentration became constant after the twelfth cycle of the MSRE.
- By using Mole to determine the effect of fuel cycling on delayed neutron precursors, satisfactory results were obtained for the delayed neutron distribution between no fuel flow in the critical state and the fuel circulation under constant volumetric flow rate. The dynamic behavior of the MSRE system presents calculations that took into account the effects of delayed neutron precursors' drift in the circulating fuel.
- For computational efficiency, delayed neutron concentration simulations are not required for noble metals and gas simulations. We can use the values to input the tabled data for the long term.

SUMMARY

The liquid–gas transport of the off-gas system can determine high-quality parameters. It accounts for salt compounds and noble gas behavior. This includes the physical and chemical processes that affect the distribution and range of movement between the various parts of the MSR system.

- We have developed for the coupling liquid–gas mass transport using Mole.
- The off-gas system of Mole is based on the fundamental correlations of liquid or gas.
- The experimental data of Henry's gas constant are not sufficient to verify the theory.
- Gas velocity and gas diffusivity theories are difficult to define; thus, the experimental results can help to validate them.
- For liquid diffusion, Wilke–Chang's distribution of noble gases is wider than that of Stokes–Einstein.
- For liquid–gas mass transport, all liquid–gas transitions tend toward a state of chemical equilibrium because Henry's gas constant is very low.
- From the concentration versus time graph, the concentration rate is dependent on the Reynolds number or diffusivity.

ACKNOWLEDGEMENTS

This work has been carried out in the framework of the NEAMS (Nuclear Energy Advanced Modeling and Simulation) program supported by the United States Department of Energy.